Implementation of Smart Materials for Actuation of Traditional Valve Technology for Hybrid Energy Systems

Saqlain Zaman [1,2], **Alba Leyva** [1,2], **Md Sahid Hassan** [1,2], **Ariztbe Valladolid** [1], **Nicolas E. Herrera** [1], **Sofia Gabriela Gomez** [1,2], **Md Shahjahan Mahmud** [1,2], **David Tucker** [3], **Comas Haynes** [4] **and Yirong Lin** [1,2,*]

1 Department of Aerospace and Mechanical Engineering, The University of Texas at El Paso, El Paso, TX 79968, USA; szaman3@miners.utep.edu (S.Z.); mhassan2@miners.utep.edu (M.S.H.)
2 Aerospace Center, The University of Texas at El Paso, El Paso, TX 79968, USA
3 National Energy Technology Laboratory, Morgantown, WV 26507, USA
4 Georgia Tech Research Institute, Atlanta, GA 30332, USA
* Correspondence: ylin3@utep.edu

Abstract: The ever-changing nature of the power industry will require the implementation of hybrid energy systems. Integration of tightly coupled components in hybrids often involves the diversion of exhaust gas flow. An innovative smart material actuation technology is proposed to replace traditional electro-mechanical actuated valve mechanisms with lighter and less expensive actuators. A shape memory alloy (SMA) spring-actuated valve was designed for high-temperature service to demonstrate the promise of smart materials in control valve applications. With SMA springs only generating a maximum force of 3.2 N, an innovative valve design was necessary. To demonstrate the concept, a 3-inch Nominal Pipe Size valve was designed, and 3D printed using the stereolithography technique. Increasing the electrical current to actuate the SMA springs reduced actuation time. The maximum current of 10 A produced the lowest actuation time of 2.85 s, with an observed maximum stroke rate of more than 100 stroke completion %/s (considering actuation open/close as 100% stroke) at the midrange. The final assembly of the valve was estimated to provide a cost reduction of more than 30% and a weight reduction of more than 80% compared to the other available automatic valves in the present market.

Keywords: shape memory alloy (SMA) spring; high-temperature valve; smart material; actuator

1. Introduction

Although valve technology is part and parcel of the modern engineering world. At the present market, any valve with a high operational temperature would be significantly expensive and heavy. The two main factors contributing to this are the high temperature-sustaining materials which are heavy, and the actuation system. This research aims to significantly reduce both the cost and the weight of the traditional valve technology by developing a valve where smart materials are implemented for the actuation. This smart material-actuated valve can potentially upgrade the present technology to a whole new level [1].

For an automated valve operating at a flow of 60 L/min in environmental temperature, the cost and weight would depend mainly on the material and actuation system. For example, a motor-driven 3-inch valve would cost around USD 776.80 with a 7.8 kg weight [2], and a pneumatic valve would be about USD 344.8 with a weight of 8.0 kg [3]. Researchers are working on developing hydraulic actuators with different composites to reduce the weight and cost of the system [4]. This research aims to generate a valve that can be actuated with smart materials such as shape memory alloy springs, which would be light in weight and cost-friendly. The cost of manufacturing the prototype 3D printed valve, including all the electronics exempt from the power source, was estimated to be approximately USD 110 with a weight of 0.5 kg, which is considerably lower.

Smart material actuators are built with materials that can respond to environmental changes and undergo a material shape change. These devices have the capability of generating the needed force to move another mechanical device. The three secular groups mainly used as smart material actuators are piezoelectric materials [5], magnetostrictive materials [6], and shape memory alloys [7–10]. Their actuation capability derives from a shape change through electric, electromagnetic, or thermal stimulation [11,12]. There are several benefits of using shape memory alloy to actuate valves. It is cheaper compared to other systems. Furthermore, the valve becomes lighter because no mechanical gearbox or motor would be required.

To demonstrate that the valve design was appropriate to control or manipulate the flow through any pipe, it was essential to manufacture the designed valve and test it in laboratory conditions. For that, AM was selected as the preferred manufacturing method. Additive manufacturing (AM), also known as three-dimensional (3D) printing, is a manufacturing method that creates physical objects from a geometrical representation by successive addition of material. A variety of AM technologies have been developed so far. For different materials such as ceramic, metal, and polymer fabrication, fused deposition modeling (FDM) [13], selective laser sintering (SLS) [14,15] powder bed fusion [16], directed energy deposition (DED) [17], binder jetting [18], direct ink writes (DIW) [19,20], and stereolithography (SLA) [21,22] can be used to create various complex structures. For this research, SLA was perfect for creating the prototype valve. The SLA method was selected because it is easy to print and modify, provides precise final resolution, and is less expensive.

In this paper, a bypass valve was designed, which would be actuated with SMA springs. To validate the effectiveness of the design, the valve was 3D printed with photo-resin in the SLA printing technique. Moreover, utilizing shape memory alloy springs, the valve was actuated, and the actuation rate was determined with the variation of electrical inputs. The feasibility of using SMA for fast response actuation to control the valve has been demonstrated. Furthermore, it is essential to point out that this design should also be suitable for high-temperature operations, where only the valve material needs to be changed to high-temperature-sustaining materials such as metal.

2. Design and Material

2.1. Material Properties and Theory of Shape Memory Alloys

Shape memory alloy's nonlinear behavior can be attributed to their internal phase transformation. The transition from one form of the crystalline structure to another creates the mechanism by which the shape change occurs. These smart materials experience two distinctive phases known as martensite (low-temperature phase) and austenite (high-temperature phase). Each phase has two different temperature values that describe the stages of actuation that shape memory springs are subjected to. These four temperatures define the start and finish transformation for each phase, as shown in Figure 1 [23,24]. One factor to notice in Figure 1 is the SMA temperature hysteresis between the martensite state and the austenite phase, showing that due to this hysteresis, the transformation from martensite to austenite will not be the same as from austenite to martensite. Table 1 shows the abbreviation from Figure 1.

Table 1. Characteristic temperatures of SMAs.

Ms	Martensite start temperature upon cooling
Mf	Martensite finish temperature upon cooling
As	Reverse transformation start temperature upon heating
Af	Reverse transformation finish temperature upon heating
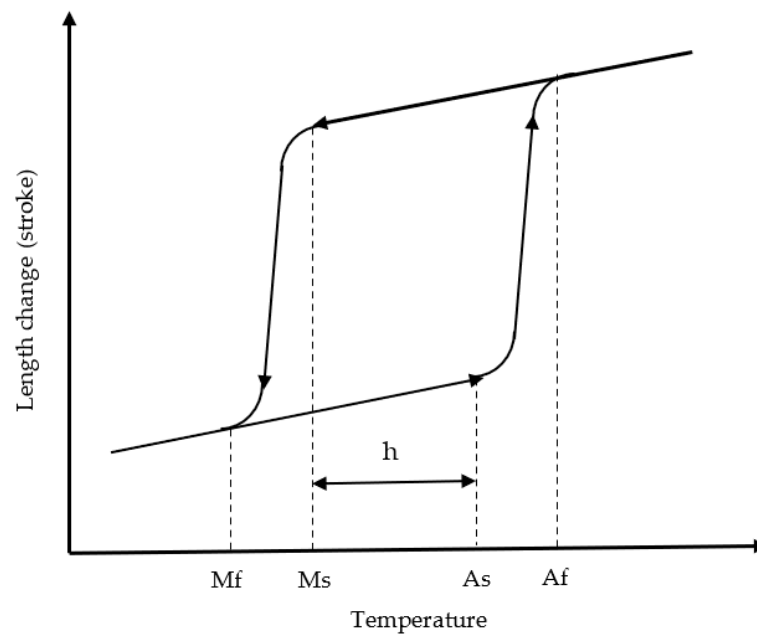
Figure 1. SMA length vs. temperature [23].

The force that the spring produces at any given deflection depends linearly on the shear modulus of the spring's material [25].

The expression for shear stress and strain relation in an SMA spring is described as:

$$\tau - \tau_o = G(\gamma - \gamma_o) + \frac{\Omega}{\sqrt{3}}(\xi - \xi_o) + \frac{\Theta}{\sqrt{3}}(T - T_o) \tag{1}$$

$$\Omega = -D\varepsilon_L (\text{ Phase Transformation Tensor}) \tag{2}$$

$$\xi = \Xi(\sigma_{eq}, T)(\text{Variable, Degree of Martensitic Transformation}) \tag{3}$$

where G is the elastic shear modulus, τ is the shear stress, γ is the strain, Ω is the phase transformation tensor, Θ is the thermoelastic tensor related to the thermal expansion of the SMA material, T is the temperature, and ξ is the internal variable describing the degree or martensitic transformation [26]. To calculate the total deflection of the shape memory alloy springs during actuation, the formulas used are those of regular springs with their specific characteristics as detailed below:

$$\text{spring max shear, } \tau_{max} = K\frac{2FR}{\pi r^2} \tag{4}$$

$$\text{Hooke's Law of Torsion determines the deformed rotation angle, } \gamma = \frac{\tau}{G} = \frac{2FR}{\pi r^3 G} \tag{5}$$

Angular deflection: measures the change in angle from both ends of the spring $\alpha = \int_0^{2\pi RN} \frac{\gamma}{r} dx = \frac{4FR^2 N}{r^4 G}$.

$$\text{total Deflection, } y = \alpha R = \frac{4FR^3 N}{r^4 G} \tag{6}$$

where K is the Wahl correction factor, which is related to the change in the coil of the spring, F is the external force created by the spring, R is the mean radius of the spring, r is the radius of the spring's wire, N is the total number of coils of the springs, and as stated before is the shear modulus. The shape memory alloy spring material used for this research is Nitinol (Nickel–Titanium). This material was chosen due to previous studies made on NiTi alloys showing better corrosion resistance, biocompatibility, high deformation recovery,

and higher electrical resistance for resistive heating in actuator applications [27]. Table 2 represents the specification of the SMA springs used.

Table 2. Properties of Nitinol shape memory alloy springs obtained from the supplier.

Wire Size	Mandrel Size	Pitch	Transition Temperature
1 mm	8 mm	1 mm	80 °C

2.2. Valve Design

The valve design is a crucial part of the project, and five factors were considered for the procedure.

1. Redirection of airflow;
2. Placement of SMA actuating springs;
3. Light rotating parts (for springs to actuate easily);
4. Leakproof;
5. SMA springs wiring.

Inspired by the butterfly valve, we designed and modified the valve with some improvements in flow control and automatic actuation. The design mainly consists of the main body (Figure 2a) with a rod (Figure 2g) and a disc (Figure 2e); the assembly of all three parts would complete the full valve (Figure 2h). After simulation in Autodesk Fusion 360 it was found that Instead of using a flat disc, a slightly curved disc was advantageous for better flow control (Figure 2f). The curvature meant that the weight of the disc would increase, which would require more force to rotate. To reduce the weight of the disc, the material was removed from the opposite side of the disc part, as shown in Figure 2e. Another major challenge was the leaks; O-rings and sealants were used at joints to make the valve leakproof. Flow control and automatic actuation improvements for compensating the friction between the rod and the main body of the valve, a modified cap was created for the top side of the valve (Figure 2c,d), where the rotating parts were connected to the static elements, and the neck of the rod was chamfered to fit an O-ring. The purpose of the cap was to create pressure from the top side to seal the leakage from the top with the O-ring. This would also reduce the amount of frictional loss. A squared chamber was designed at the top of the valve, which includes actuation stoppers and places for SMA springs installation, Figure 2b. The sidebars act as the stoppers, stopping the valve in on and off positions. One side of the springs would be directly connected to the rod, which is connected to the disc, and the other side would be attached to the side holes. The spring would actuate the valve when applied with electricity from the D.C. power supply. In Figure 2i, the voltage applied to both SMA springs is denoted (A). Therefore, SMA will contract and the normal springs will change to their elongated position. In the same manner, the disc inside the pipe will turn depending on the displacement of the SMA spring (A) opening the outlet and allowing flow throughout the pipe system.
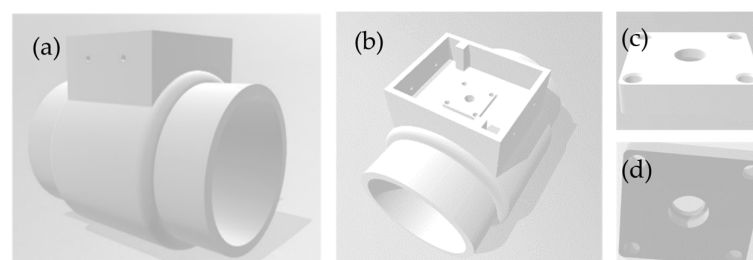
Figure 2. *Cont*.
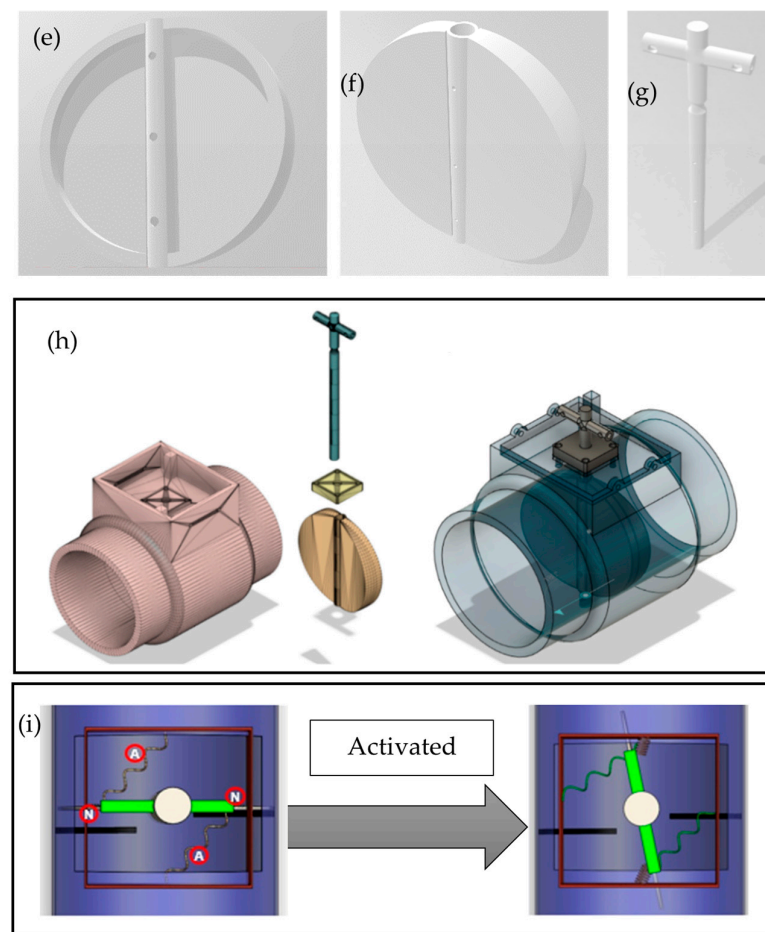
Figure 2. Design of the valve consisting of (**a**) the main body of the valve, (**b**) the top side of the main body, (**c,d**) the top and bottom side of the top cap, respectively, (**e,f**) both sides of the disc, (**g**) the actuation rod, (**h**) the full valve setup, and (**i**) spring connection and activation system.

2.3. Boundary Conditions

To prove that the design is practically feasible, boundary conditions for experimenting were designed with considerations for the cost, available environment, and space for the experiment. For the testing of the valve mount, it was connected to a 3-inch PVC pipe on both ends, with a Y-type connection as shown in Figure 3. The test was completed at room temperature with a flow of 60 L/min compressed air. Flow meters were placed on the inlet and each outlet to measure the actual flow and how much the valve can redirect the flow.
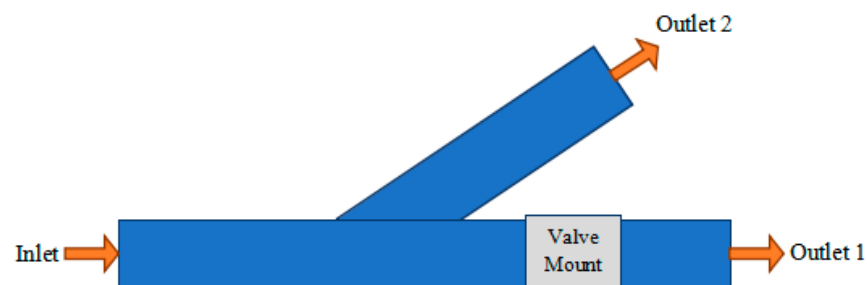
Figure 3. Flow diagram for compressed air.

3. Experimental Section

3.1. 3D Printing of the Valve

For 3D printing of the designed valve, Formlabs Form 3 stereolithography 3D printer (Formlabs, Chicago, IL, USA) was used. As the SMA springs actuate with a temperature

up to 80 °C, clear resign (Formlabs, Chicago, IL, USA), which can sustain that temperature, was utilized to fabricate all specimens, and standard printing parameters were used. After fabrication, the model was subjected to a post-curing process during which UV light (405 nm) was applied for 180 min.

3.2. Instruments

A 26-gallon oil-free air compressor (Kobalt, Lowe's, Mooresville, NC, USA) was used for experimental testing to generate the required airflow. For measuring the air flow rate at the beginning and end of the PVC pipes, flow meters (Cole Palmer, Chicago, IL, USA) were connected. The joints are sealed with sealant to prevent any leakage. SMA springs (Kellogg's Research Lab, New Boston, NH, USA) were used to actuate the valve and a 100 W power capacity DC power supply with a 60 V/5 A rating (model 9110, B&K Precision Corporation, Yorba Linda, CA, USA) was utilized. Digital Scale (Polychrome gear, New York, NY, USA) was used to measure the force generated by each spring.

3.3. Testing Setup

To prove that the SMA springs can actuate a valve in practical applications, it was essential to test it out in a particular flow. The compressor was used to generate the flow as the starting point. It was connected to an airflow meter with a flexible pneumatic pipe and connector. The air flows through the airflow meter into a 3-inch Y-type PVC pipe. One end of the Y-type line (outlet 1) is connected to the 3D-printed valve with a flow meter before finally letting the air into the environment. The other end (outlet 2) was directly related to a flow meter. Sealants were used in all solid joints to reduce leakage from joints, and jubilee clamps were used on the flexible pipes. The springs were mounted on top of the valve as per design. A D.C. power supply was directly connected to the springs to actuate the springs. Wirings from the power supply were connected through a 2-way switch to the springs. The two-way switch is used to provide valve actuation commands. The final setup is shown in Figure 4.
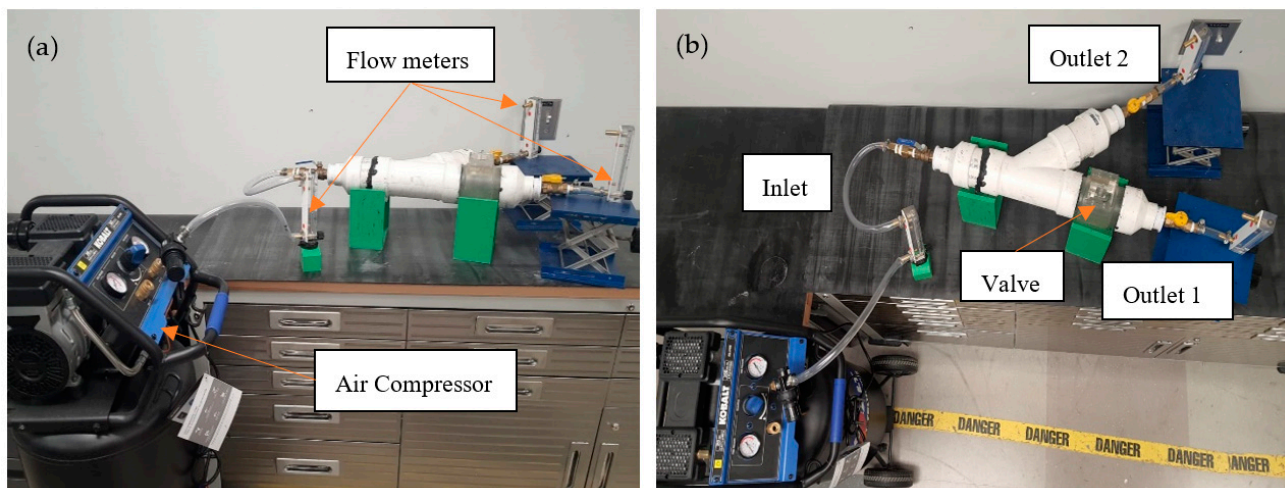
Figure 4. Experimental setup of the valve (**a**) side view, (**b**) top view.

3.4. Experimental Method

3.4.1. SMA Spring Compression Time

To determine the time required for the SMA spring compression, the springs were first stretched from an initial length of 13 mm to 42.5 mm. Then DC electrical power was supplied, connecting positive and negative lines at both ends of the SMA spring to the power supply. This electrical supply generates heat in the spring. The SMA spring then starts to shrink and return to its original length. The time required for the spring to compress to its original form was noted. Furthermore, keeping the voltage constant,

variable electrical current was supplied to the SMA spring to find the relation between electrical current and compression time.

3.4.2. Spring Load Capacity Test

Determining how much force each spring could generate is important to determine the SMA spring's capability to actuate the valve. To check that, initially, the spring was stretched from an initial length of 13 mm to a length of 42.5 mm. Then one end of the spring was fixed with a clamp, and the other was hooked with a weighing scale which was also fixed and tared to zero (Figure 5). Then DC electrical power was supplied, connecting positive and negative lines at both ends of the SMA spring to the power supply. The values are shown on the scale in kilograms with the spring compression. Later, it was converted into Newtons (force).
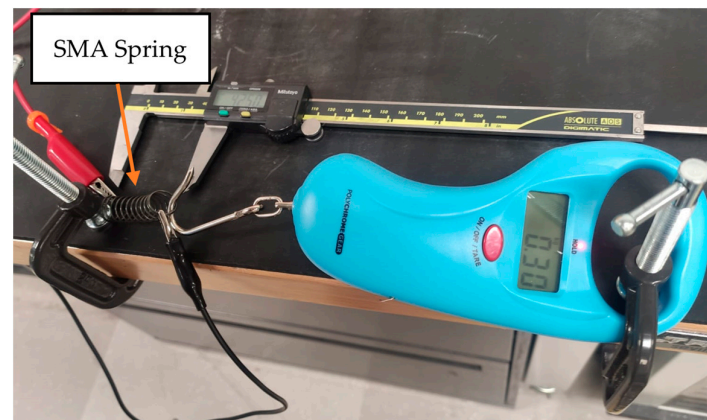
Figure 5. Setup for SMA spring load capacity test.

3.4.3. Actuation Time and Flow Output Test of the Valve

For practical implementation of the design, it was essential to determine the actuation time and flow control with experimental testing. For that, the flow was generated with the compressor and measured through the flow meters. Two SMA springs were used for the actuation of the valve. One for opening and one for closing. The springs were powered with two D.C. power supplies. The actuation of the valve was controlled with a two-way switch. The actuation time was checked with different electrical outputs from the power supply. Furthermore, the flow redirection results were collected when the valve was in fully open and closed conditions.

4. Result and Discussion

4.1. Mechanical Properties of SMA Springs

The valve's response time depends mainly on the time required for the springs to shrink to their original shape when applied with electrical current. This was quantified by keeping the voltage constant at 5 V with a varying current, and the results are shown in Figure 6a. It can be interpreted from the graph that, with the increase in current supply, the amount of time required for springs to compress decreased simultaneously. With a maximum of 10 A, the compression time was 1.36 s. The amount of force the springs can generate is also significant, as the springs would have to rotate the disc with the rod at high flow rates inside the pipes. This was also determined while keeping the voltage constant at 5 V with a varying current, and the results are shown in Figure 6b. Each of the springs generated a maximum 3.2 N force. The amount of time required to reach the maximum force varied with the amount of supplied current and decreased with the current increment. Furthermore, when comparing Figure 6a,b, they show almost similar trends. So, the time a spring takes to return to its original shape after being stretched is the same as the time for reaching the maximum force spring can generate.
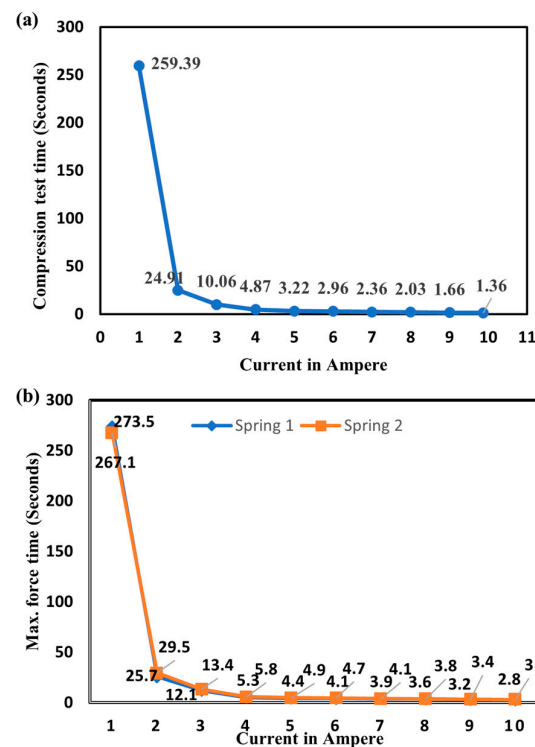
Figure 6. (**a**) Time vs. current graph for compression of spring and (**b**) time vs. current graph for reaching maximum force generated by springs.

4.2. Actuation of 3D Printed Valve with SMA Springs

After the characterization of SMA springs, the next experiment is to validate the use of SMA to actuate the designed valve. So, the actuation was tested with different electrical inputs. For the opening and closing of the valve, it needed to rotate from 0° to 90°. So, it was marked with a 15° interval, and the time required to reach each checkpoint was measured. The results of actuation speed with a constant voltage of 5 V and variation of electrical currents from 2–10 A are shown in Figure 7. It must be noted that it was not possible to actuate the valve with less than 2 A because the springs could not generate enough force with low electrical inputs, and the actuation time for 2 A was significantly high with more than 120 s required for actuation (Figure 7a). Furthermore, the actuation time gradually decreased with the increase in current, with the lowest time noted being 2.85 s with an electrical current of 10 A (Figure 7b). However, with the rise in current, the life expectancy of SMA springs drops [28]. Keeping that in mind, the maximum current was chosen to be 10 A. It was also pointed out that although the actuation of the valve reduced with increments of electrical inputs, it did not vary significantly after 7 A, with 7 A taking 4.35 s. However, the actuation time of the valve was slower compared to the compression time. The reason was that the springs had to maneuver the weight of the rod and disc and actuate the valve against the airflow. There was one more noticeable characteristic from Figure 7. The actuation time is comparatively slower during the starting and ending 30° compared to the other middle sections. That is because it took a little time to generate the heat needed for SMA springs to start actuation. As shown in Figures 7 and 8, the response time performance of the valve is not linear with respect to position. At the saturation points, the valve slows to a stroke completion speed is 20%/s. In the midrange, the valve response with stroke completion speed as high as 110%/s. In applications requiring minimum flow, this feature could be attractive. Regardless, further optimization of the material and valve design would likely provide an improved response over those reported herein.
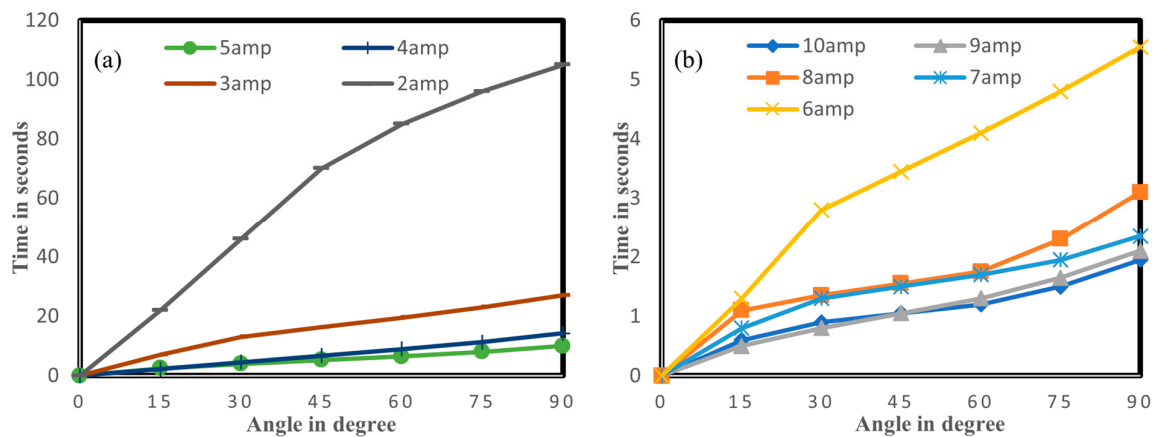
Figure 7. Actuation time vs. angle traveled by the valve for 5 V constant voltage and current of (**a**) 2–5 A and (**b**) 6–10 A.
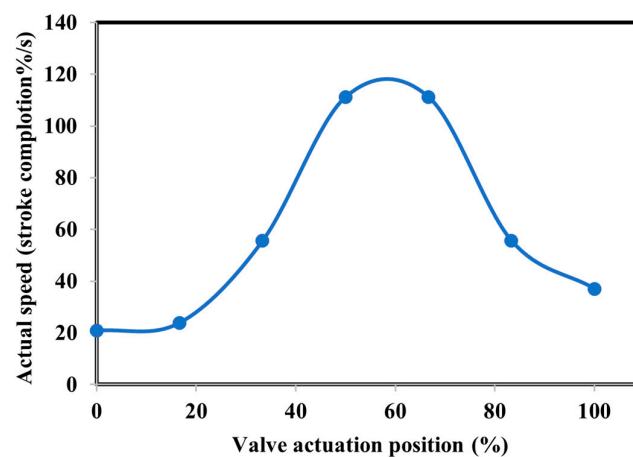
Figure 8. Actuator response stroke rate as a function of valve position for the 10 A current.

4.3. Flow Control of the 3D Printed Valve

Lastly, to validate that the valve can be practically used to control the airflow using the setup as shown in Figure 4, a set of experiments were carried out to demonstrate the feasibility of controlling the airflow. In this experiment, inlet flow was set at 60 L/min, while the valve in outlet one was controlled to open and close upon electrical actuation. The data obtained from each flow meter at both the open and closed positions of the valve are shown in Table 3.

Table 3. Showing the amount of flow redirected by the actuation of the valve.

Valve Condition	Inlet Flow	Outlet 1 Flow	Outlet 2 Flow
Fully Open	60 L/min	28 L/min	28 L/min
Fully closed	60 L/min	6 L/min	46 L/min

When the valve was fully open, the inlet flow of 60 L/min was divided equally within both outputs. There was a 4 L/min airflow leakage even though the leaks were sealed with sealants at the pipe joints and an O-ring at the top of the valve. This was mainly because of the PVC pipes, which were unsuitable for handling compressed air [29]. When the valve was fully closed, the flow decreased to 6 L/min in outlet one and increased up to 46 L/min in output 2. The reason the flow was not entirely zero L/min in output 1 was that when the disc was in a closed position inside the valve, it did not fully cover the entire cross-section area as there were still some small gaps at the edges inside the valve, so the air leaked through those leaks and showed a flow of 6 L/min at output 1.

Furthermore, the system leakage increased from 4 L/min to 8 L/min. The main reason was that when the valve was closed, the pressure inside the PVC pipe increased, so leakages also increased for the total system due to increased pressure. However, it can be seen from Table 3 that a high amount of flow was redirected when the valve was actuated from the open to closed position with the SMA springs. To further improve the leakage situation and for high-temperature applications, the valve can be manufactured with stainless steel for future studies.

5. Conclusions

Smart material has produced marvelous results in different actuating technology in recent years. In this research, SMA springs were implemented as actuators in valve technology to reduce weight and cost. The spring compression time depends on the supplied electrical inputs, and with the increase in electrical current, it reduces extensively. As the amount of force generated was not very high so the rod and disc were designed in such a way that it would compensate for that, and the valve would actuate with this lower force. A valve model was evaluated with a 3D-printed valve operating with an airflow of 60 L/min at room temperature. The fastest actuation time recorded was around 2.85 s with 5 V and 10 A of D.C. electrical supply. The testing results have shown that the SMA can be integrated into a valve system to control the airflow upon actuation. The manufacturing cost for the designed valve was approximately USD 110, with a weight of roughly 0.5 kg. It can be said that the final price would be around USD 200 [30]. Both price and weight were considerably lower, with the price being 30% less and weight more than 80% less compared to the other available automatic valves in the present market.

Author Contributions: Conceptualization, S.Z. and A.L.; investigation, S.Z., A.V., A.L., M.S.H., N.E.H. and M.S.M.; writing—original draft preparation, S.Z.; writing—review and editing, M.S.H., S.G.G., Y.L., D.T. and C.H.; supervision, Y.L.; project administration, D.T.; funding acquisition, C.H. All authors have read and agreed to the published version of the manuscript.

Funding: This work has received funding from the Department of Energy with the Partnership for Research Education Consortium in Ceramics and Polymers (PRE-CCAP) program and the Consortium of Hybrid Resilient Energy Systems (CHRES) program. The authors gratefully acknowledge the support from the Department of Energy (grant No: DE-EE0009137, DE-NA-0004051, and DE-NA0003982).

Data Availability Statement: The datasets used and analyzed during the current study are available from the corresponding author upon reasonable request.

Conflicts of Interest: On behalf of all the co-authors of this manuscript, the author would like to mention that we have no conflicts of interest to disclose.

References

1. Burman, A.; Møster, E.; Abrahamsson, P. On the Influence of Functional Materials on Engineering Design. *Res. Eng. Des.* **2000**, *12*, 39. [CrossRef]
2. 1/2 Description Specifications Accessories Data Sheets CAD Video Repair Parts. Available online: https://www.valworx.com/product/electric-actuated-butterfly-valve-3-lug-epdm-12-or-24-vdc/electric-actuated-butterfly-valves-lug-style-on-off?utm_source=google&utm_medium=surfaces&utm_campaign=Surfaces (accessed on 14 September 2022).
3. In Air Actuated Butterfly Valve, Wafer, EPDM | Valworx. Available online: https://www.valworx.com/product/air-actuated-butterfly-valve-3-waferepdmdouble-acting/air-actuated-butterfly-valves-wafer/ (accessed on 27 September 2022).
4. Lubecki, M.; Stosiak, M.; Skačkauskas, P.; Karpenko, M.; Deptuła, A.; Urbanowicz, K. Development of Composite Hydraulic Actuators: A Review. *Actuators* **2022**, *11*, 365. [CrossRef]
5. Mohith, S.; Upadhya, A.R.; Navin, K.P.; Kulkarni, S.M.; Rao, M. Recent trends in piezoelectric actuators for precision motion and their applications: A review. *Smart Mater. Struct.* **2020**, *30*, 013002. [CrossRef]
6. Apicella, V.; Clemente, C.S.; Davino, D.; Leone, D.; Visone, C. Review of Modeling and Control of Magnetostrictive Actuators. *Actuators* **2019**, *8*, 45. [CrossRef]
7. Ruth, D.J.S.; Dhanalakshmi, K.; Nakshatharan, S.S. Bidirectional angular control of an integrated sensor/actuator shape memory alloy based system. *Measurement* **2015**, *69*, 210–221. [CrossRef]
8. Renata, C.; Kalairaj, M.S.; Chen, H.M.; Lau, G.K.; Huang, W.M. Buttons on Demand Sliding Mechanism Driven by Smart Materials and Mechanical Design. *Actuators* **2021**, *10*, 251. [CrossRef]

9.   Rajagopalan, R.; Petruska, A.J.; Howard, D. A Bi-State Shape Memory Material Composite Soft Actuator. *Actuators* **2022**, *11*, 86. [CrossRef]

10.   Kostov, M.; Todorov, T.; Mitrev, R.; Kamberov, K.; Nikolov, R. A Study of a Bistable Reciprocating Piston Pump Driven by Shape Memory Alloys and Recuperative Springs. *Actuators* **2023**, *12*, 90. [CrossRef]

11.   Straub, F.K.; Merkley, D.J. Design of a smart material actuator for rotor control. In *Smart Structures and Materials 1995: Smart Structures and Integrated Systems*; SPIE: Bellingham, WA, USA, 1997.

12.   Cortez-Vega, R.; Chairez, I.; Luviano-Juárez, A.; Feliu-Batlle, V. A hybrid dynamic model of shape memory alloy spring actuators. *Measurement* **2018**, *114*, 340–353. [CrossRef]

13.   Popescu, D.; Zapciu, A.; Amza, C.; Baciu, F.; Marinescu, R. FDM process parameters influence over the mechanical properties of polymer specimens: A review. *Polym. Test.* **2018**, *69*, 157–166. [CrossRef]

14.   Hassan, S.; Billah, K.M.M.; Hall, S.E.; Sepulveda, S.; Regis, J.E.; Marquez, C.; Cordova, S.; Whitaker, J.; Robison, T.; Keating, J.; et al. Selective Laser Sintering of High-Temperature Thermoset Polymer. *J. Compos. Sci.* **2022**, *6*, 41. [CrossRef]

15.   Chavez, L.A.; Ibave, P.; Hassan, S.; Hall-Sanchez, S.E.; Billah, K.M.M.; Leyva, A.; Marquez, C.; Espalin, D.; Torres, S.; Robison, T.; et al. Low-temperature selective laser sintering 3D printing of PEEK-Nylon blends: Impact of thermal post-processing on mechanical properties and thermal stability. *J. Appl. Polym. Sci.* **2022**, *139*, 52290. [CrossRef]

16.   Sun, S.; Brandt, M.; Easton, M. Powder bed fusion processes. In *Laser Additive Manufacturing*; Elsevier BV: Amsterdam, The Netherlands, 2017; pp. 55–77.

17.   Ahn, D.-G. Directed Energy Deposition (DED) Process: State of the Art. *Int. J. Precis. Eng. Manuf. Technol.* **2021**, *8*, 703–742. [CrossRef]

18.   Ziaee, M.; Crane, N.B. Binder jetting: A review of process, materials, and methods. *Addit. Manuf.* **2019**, *28*, 781–801. [CrossRef]

19.   Del-Mazo-Barbara, L.; Ginebra, M.-P. Rheological characterisation of ceramic inks for 3D direct ink writing: A review. *J. Eur. Ceram. Soc.* **2021**, *41*, 18–33. [CrossRef]

20.   Regis, J.E.; Renteria, A.; Hall, S.E.; Hassan, S.; Marquez, C.; Lin, Y. Recent trends and innovation in additive manufacturing of soft functional materials. *Materials* **2021**, *14*, 4521. [CrossRef]

21.   Hassan, S.; Chavez, L.A.; Chou, C.-C.; Hall, S.E.; Tseng, T.-L.; Lin, Y. Mechanical response of shape-recovering metamaterial structures fabricated by additive manufacturing. *Mater. Res. Express* **2021**, *8*, 115801. [CrossRef]

22.   Yin, R.; Huang, Q.; Yang, H.; Lu, L.; Cao, L.; Ji, W.; Jiang, S.; Luo, Y.; Liu, F.; Sun, J.; et al. Integrated-optics pressure sensor with improved range and sensitivity based on a SiO_2 arrayed waveguide grating (AWG) and a 3D printed stereolithography resin module. *Measurement* **2021**, *183*, 109781. [CrossRef]

23.   Anadón, J.R.S. Large Force Shape Memory Alloy Linear Actuator. Master's Thesis, University of Florida, Gainesville, FL, USA, 2002.

24.   Jacobsen, A.; Kristjánsdóttir, N.B. Shape Memory Alloys. *Annu. Rev. Mater. Sci.* **1988**, *18*, 25–45.

25.   Ma, J.; Huang, H.; Huang, J. Characteristics analysis and testing of SMA spring actuator. *Adv. Mater. Sci. Eng.* **2013**, *2013*, 823594. [CrossRef]

26.   Liang, C.; Rogers, C.A. Design of shape memory alloy springs with applications in vibration control. *J. Intell. Mater. Syst. Struct.* **1997**, *8*, 314–322. [CrossRef]

27.   Formentini, M.; Lenci, S. An innovative building envelope (kinetic façade) with Shape Memory Alloys used as actuators and sensors. *Autom. Constr.* **2018**, *85*, 220–231. [CrossRef]

28.   Singh, H.; Juikar, P.; Tiwari, T.N.; Lad, B.K.; Palani, I.A. Failure diagnosis & reliability assessment of NiTi shape memory alloy spring for micro-Actuators. In Proceedings of the 2015 International Conference on Robotics, Automation, Control and Embedded Systems (RACE), Chennai, India, 18–20 February 2015; pp. 1–6. [CrossRef]

29.   Using PVC Pipe for Compressed Air. Available online: https://compressors.cp.com/en-us/expert-corner/blog/pvc-pipe-why-you-should-not-use-pvc-piping-for-your-compressed-air-system (accessed on 6 August 2022).

30.   Widyatama, U.; Rachman, Y.; Abdul, R.; Rachmat, H. Calculation Analysis of Cost of Production in Determining Product Selling Price. Available online: www.solidstatetechnology.us (accessed on 27 September 2022).